Chorus waves in the Van Allen belts during violent geomagnetic storms

I. Cannon,[1] supervised by N. Meredith,[2] and S. Glauert[2]

[1] Churchill College, Cambridge University, England
[2] British Antarctic Survey, National Environment Research Council, Cambridge, England

ABSTRACT

Chorus waves are a type of electromagnetic wave in the Van Allen belts. These waves can accelerate electrons to high energies, presenting a risk for orbiting satellites. Due to the rarity of large geomagnetic storms, we have very few measurements of chorus waves during periods of high geomagnetic activity. Here we describe how existing satellite measurements were used to predict chorus wave behaviour during these periods. Our predictions are in good agreement with previous observations, for example, the majority of wave power is on the morning side of the Earth, and the chorus wave spectra show a dip in intensity at half of the gyrofrequency. From the predicted wave power, we can calculate the rates of electron energy and pitch angle diffusion, for use in simulations of geomagnetic storms.

1. Introduction

The Van Allen radiation belts were first detected using a Geiger counter aboard Explorer 1, the third man-made satellite [*Van Allen,* 1959]. As of June 2016, there are around 1000 operational satellites in orbits which come into contact with the belts [*SIA,* 2016]. Large storms in the Van Allen belts are rare but devastating. For example, as stated in [*Horne et al.,* 2013(1)], "Between 23 October and 6 November 2003, 47 satellites reported malfunctions, and the US $640 million Midori 2 was a total loss." This coincided with a large ejection of high energy particles from the Sun, and significant changes in the radiation belts.

This project aims to obtain realistic maps of chorus wave intensity during active solar conditions. The maps will be used in forecasting geomagnetic storms. See [*Horne et al.,* 2013(1)] for an outline of the SPACECAST space weather forecasting system.

We used the IDL programming language for data handling and plotting. IDL was chosen as it well suited for manipulating large data sets. Also, its popularity in astronomy and atmospheric physics means there is a wealth of code which can be adopted and modified.

2. Terminology

chorus wave A right-hand circularly polarized electromagnetic wave in the Van Allen belts. Chorus waves are produced by moving electrons, and can transfer energy to other electrons in the plasma. Named as such because they produce a noise like the dawn chorus when converted into a sound signal. Also known as whistler mode waves.

gyrofrequency, f_{ce} The rotational frequency of an electron in a magnetic field, also known as the cyclotron frequency. The range $0 - 0.5 f_{ce}$ is referred to as the lower band, and $0.5 - 1 f_{ce}$ is referred to as the upper band.

magnetic drift invariant, L^* A geomagnetic coordinate which denotes distance from the centre of the Earth, defined by:

$$L^* = -\frac{2\pi k_0}{\Phi R_E}.$$

Where k_0 is the magnetic dipole moment of the Earth, R_E is the radius of the Earth, and Φ is the magnetic flux enclosed by a circle of radius L^* in the equatorial plane. $L^* = 1$ roughly corresponds to one Earth radius.

magnetic local time, MLT A geomagnetic coordinate which is analogous to longitude on the Earth's surface. The MLT of a point in space is the angle created by bisecting a plane containing the Earth's axis and the point, with a plane containing Earth's axis and the Sun. The angle is expressed in hours and minutes, with 360° corresponding to 24 hours. E.g., for a point between the Earth and the Sun, the MLT is 12:00.

planetary K-index, K_p A scale of geomagnetic activity which takes a value in the range 0-9. Values greater than five indicate a geomagnetic storm. The index depends on the size of fluctuations in the horizontal component of Earth's magnetic field, measured at 13 observatories around the poles.

plasmapause The outer boundary of the plasmasphere; a region surrounding the Earth which contains a dense plasma of low energy electrons.

3. Measured Chorus Waves

Chorus wave data was taken from the SPACECAST wave database. This includes measurements dating from 1981 to 2014, made by a number of satellites; Dynamics Explorer 1, CRRES, Cluster 1, Double Star TC1, THEMIS, and The Van Allen Probes. Figure 2 shows the average measured chorus wave intensity in the equatorial plane. Notice that there are very few measurements during periods of high activity ($8 \leqslant K_p < 9$).

The data was split into nine frequency bins in the range 0 to $1 f_{ce}$, and seven latitude bins in the range $-42°$ to $-42°$. Throughout this report, the same statistical methods will be applied to all 63 latitude-frequency bins. However, the highest chorus intensities are observed at the equator and in the middle of the lower frequency band. Higher intensity chorus waves cause greater

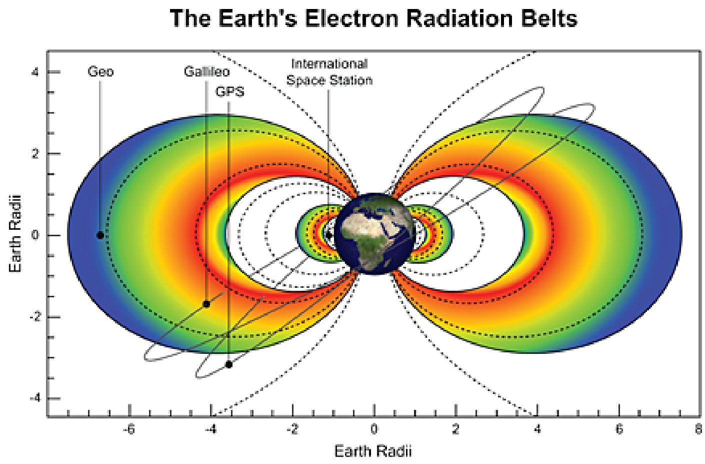

Fig. 1: The inner and outer radiation belts. Orbits of various satellites are labelled, including geostationary orbit (Geo). Figure courtesy of N. Meredith, with permission.

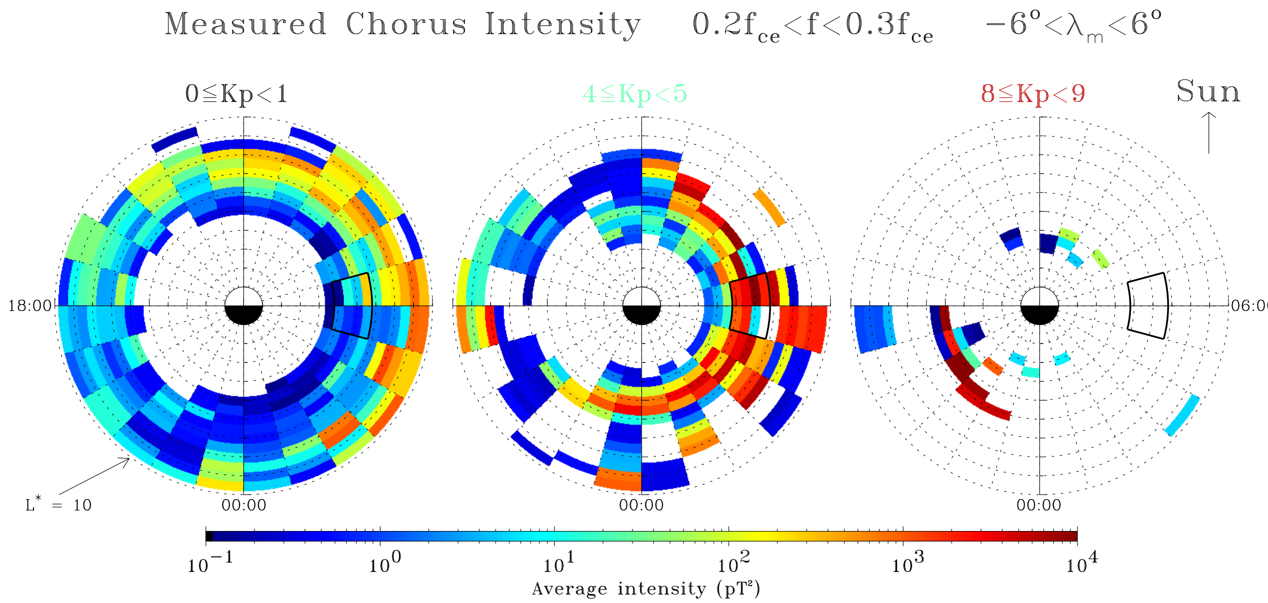

Fig. 2: Measured chorus intensity during periods of low solar activity (left), moderate solar activity (mid), and very high solar activity (right). These measurements were made within 6° of the equator. Notice the lack of data at high activities.

electron pitch angle and energy diffusion rates, often leading to a larger flux of relativistic electrons. Hence most of our plots will consider the $-6^\circ < \lambda < 6^\circ$ latitude and $0.2 < f/f_{ce} < 0.3$ frequency.

The data was also split into bins of size $0.5L^*$, and one hour of magnetic local time. Giving a high enough resolution to capture patterns in the chorus waves, but also ensuring that most bins contain enough measurements to provide a reliable average.

The position of the plasmapause was estimated as the radius at which the measured chorus wave intensity drops off [*Kersten*, 2016]. However, for $K_p \geqslant 8$, there is not enough data to ascertain a drop off. Instead we assumed the plasmapause moves in to $L^* = 1.3$, as reported in [*Baker et Al,* 2004]. All measurements taken inside the plasmapause were assumed to be non chorus and discarded.

4. Extrapolating to Higher Activities

In order to determine the chorus wave intensity during periods of high activity, we applied a best fit technique to the data in each spatial bin. Figures 3a and 3b both correspond to the bins outlined by a black box in Figure 2. The diamond shaped points in Figure 3a represent the *mean* intensity in each K_p bin. These values are used to calculate the current SPACECAST diffusion coefficients. When finding the best fits (solid and dotted lines), each point was weighted according to the number of samples.

In Figure 3b, the fitting algorithm used the *individual* intensity measurements to calculate a best fit. Notice how the fitted curves are very similar in Figures 3a and 3b. We chose to fit to each individual point (Fig. 3b), as this method takes the spread of data into account. For example, the measurements in some of the K_p bins are spread over four orders of magnitude, and it is important these bins have less weighting than a bin with the same number of measurements but a smaller spread.

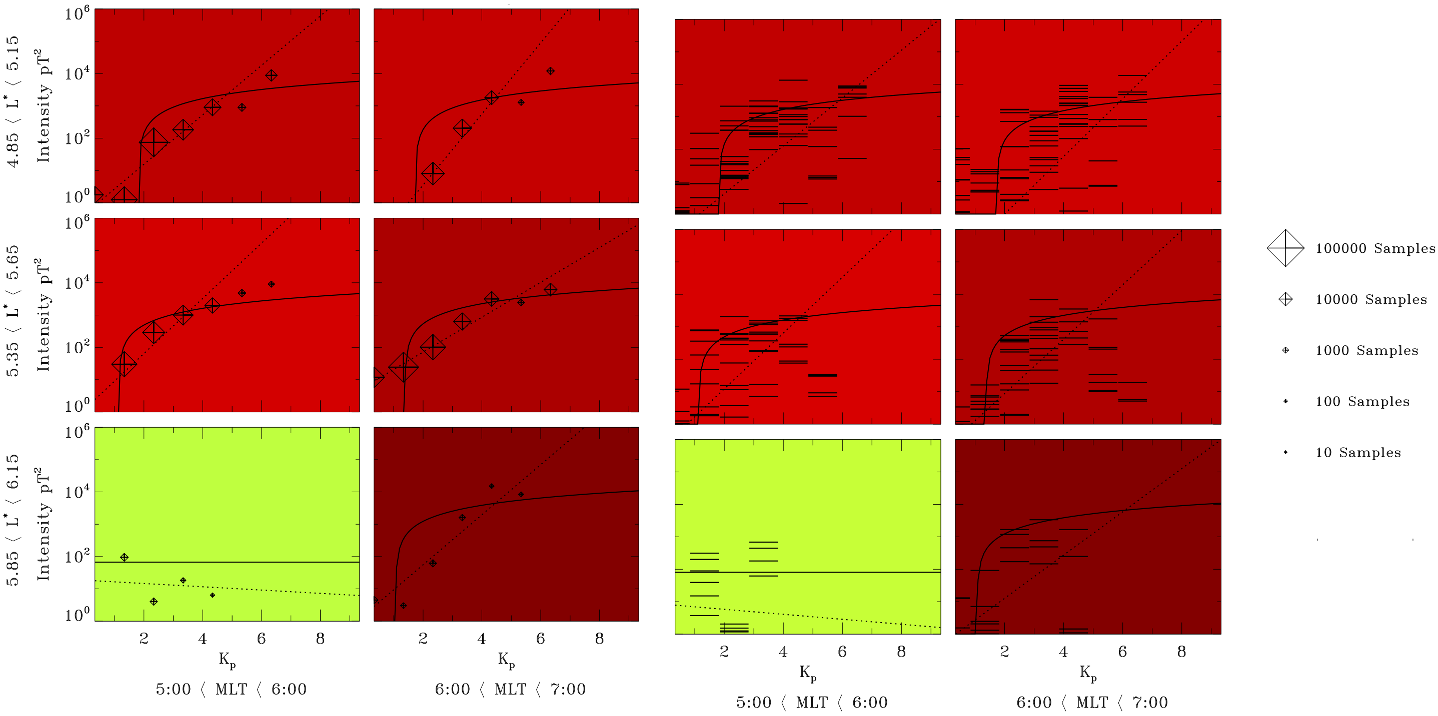

(a) Fits to the mean intensity in each K_p bin. The area of each point is proportional to the number of measurements.

(b) Fits to the individual measured intensities in each K_p bin.

Fig. 3: Extrapolating the chorus wave intensity data. Dashed lines show exponential fits and solid lines show linear fits. The wave intensity is shown on the y-axis with a logarithmic scale, hence linear fits appear curved. Each plot is coloured according to the $8 \leqslant K_p < 9$ chorus intensity, predicted by the linear fit.

There is no known analytical relationship between K_p index and chorus intensity, so various fitting functions were investigated. Exponential fits (shown as dotted lines in Figure 3) gave a close fit at low K_p, but predicted unphysically high intensities for $K_p \geqslant 7$. Linear fits (solid curves in Figure 3) predicted intensities within the range of previous measurements and proved much closer to the data at high K_p. We chose linear fits, as it is the high activity predictions which will be used to calculate diffusion coefficients.

Figure 4 shows the values of the fitted lines at $K_p = 0.33, 4.33$, and 8.33. Intensities are higher on the morning side (00:00 to 12:00), which is in agreement with the measured data in Figure 2. However, we see bins with negative intensity, shown in dark blue. We also see anomalous bins, which are hundreds of times greater than their neighbors. These problems are tackled in the following section.

5. Eliminating the Poorest Fits

Applying a best fit to all spatial bins gave just over 58 000 fitted lines. For each line, our procedure counted the number of K_p bins containing more than three measurements. We shall refer to this as the *number of points* in the spatial bin. For example, there are seven K_p bins with more than three measurements (seven points) in the top left plot in Figure 3b. Fits to large numbers of points will provide the most reliable extrapolations. As shown by Figure 5, roughly 30 000 best fit lines were created using two or more points, and only 1000 using eight or more. We decided to eliminate all fits with fewer than four points, as this removed the anomalous bins from the plot, without losing too much data.

Negative intensity bins were set to 0.1 pT^2, as this is a typical chorus intensity seen during quiet periods, such as the evening side of the $0 \leqslant K_p < 1$ plot in Figure 2.

6. Filling Empty Bins

The bins containing no data were filled using an average intensity from surrounding bins. We used an iterative process;

1. Copy wave intensities to a temporary array.
2. Unfilled bins in the temporary array are assigned a value of infinity.
3. Count the number of filled bins in a region surrounding an unfilled bin. This region extends three bins out to higher L^*, and one bin inward to lower L^*, as outlined in black on the leftmost plot in Figure 6.
4. If at least two of the four surrounding bins are filled, then calculate their mean intensity from the temporary array. Ignore any infinite values using the NAN keyword in IDL. Weight the mean according to the number of measurements in each bin. Fill the corresponding unfilled bin in the original array with this mean intensity value.
5. If fewer than two surrounding bins are filled, then leave it unfilled.
6. Repeat steps 3 to 5 for all unfilled bins in the original array.

This process was repeated seven times, the first two repeats are shown in Figure 6. Newly filled bins are highlighted with a white line. When calculating means, bins filled by the iterative process were given a weighting of 12. This value was chosen as it is the minimum number of measurements used to make each line of best fit.

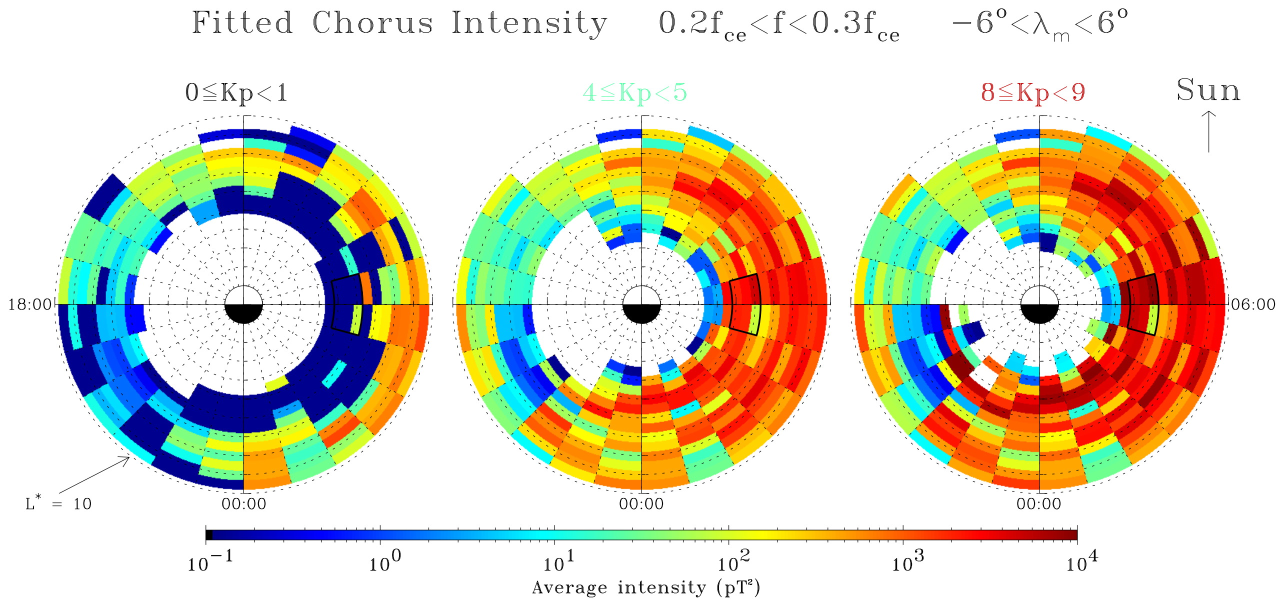

Fig. 4: Chorus intensity maps made using a linear fit in each spatial bin. Negative (uphysical) values are shown in dark blue. The bins surrounded by a box correspond to the plots in Figure 3b.

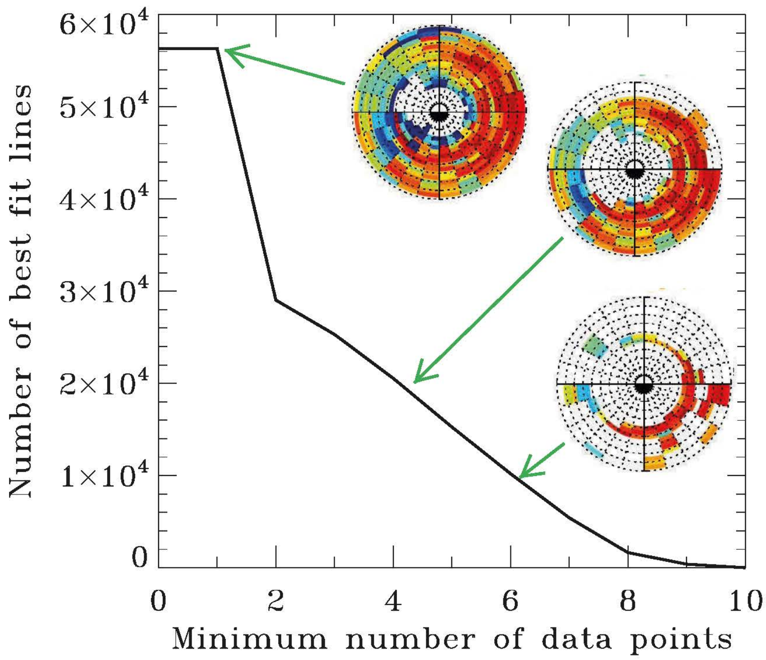

Fig. 5: Plot to show the number of best fit lines created from at least n data points. n increases from zero to ten along the x-axis. Intensity maps when $n = 2, 4, 6$ are shown. Notice when $n = 6$, most of the remaining fits lie at $L^* \approx 5$. This corresponds to the apogee of the Van Allen probes, where a large number of measurements have been taken.

When K_p increases, the chorus waves tend to move inwards. This is the reason we chose an asymmetrical averaging region mentioned in step three. The region extends further outwards than inwards, hence bins are filled using mainly intensity values from larger L^*.

Next, the maps were smoothed by replacing the intensity in each bin with the mean value in the bin itself, and all six of the adjoining bins. I.e., the bins at ±1 hour of MLT, $\pm 0.5L^*$, and $\pm 6°$ of latitude. This removed any abnormally high intensity bins in calm areas, albeit with a reduction in spatial resolution. Finally, all bins inside the plasmapause were set to zero intensity.

7. Results and Discussion

The final results (Figure 7) show the majority of chorus wave power on the morning side, which is in agreement with the mea-

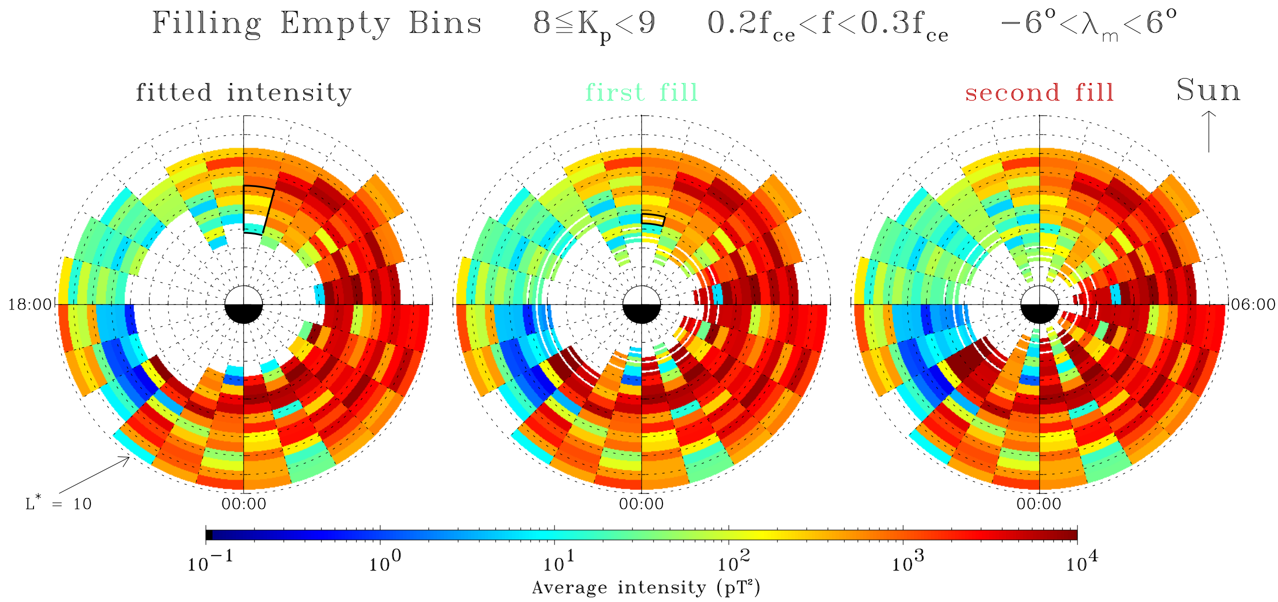

Fig. 6: Plot to show the first two repeats of the filling process. Newly filled bins are marked with a white line. The single outlined bin in the central plot was filled using values from the five outlined bins in the left plot.

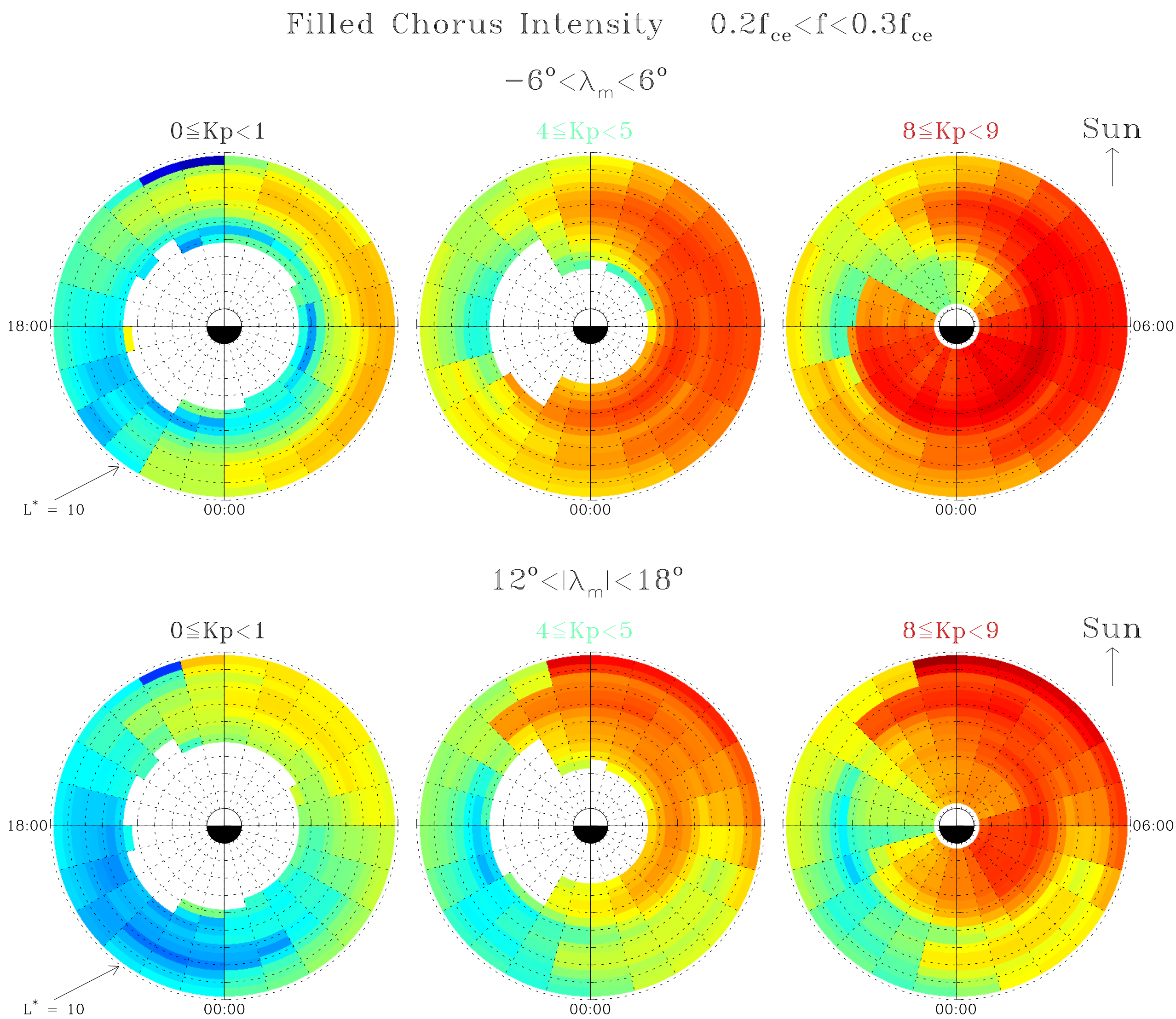

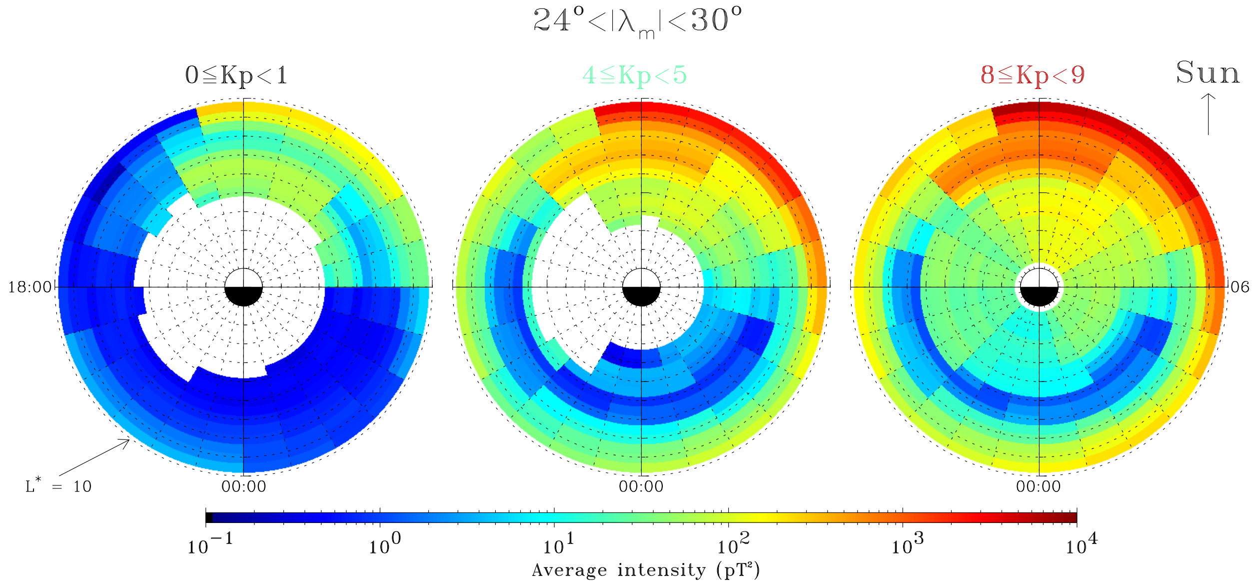

Fig. 7: Plots to show the final extrapolated chorus wave intensities. As K_p increases, we see intensities increase, especially on the morning side. We also see the plasmapause move inwards. At greater latitudes (down the page), high intensity waves are found at later MLT. We believe these intensity values are a realistic and comprehensive description of chorus waves in the Earth's radiation belts.

sured waves in Figure 2. Figure 7 also shows the wave power moving to later MLT at higher latitudes. This can be explained by chorus wave theory; the bulk of low energy electrons are on the night side, and these absorb chorus waves, preventing the waves from propagating to higher latitudes [*Bortnik et al.,* 2007].

Solar electrons are injected into the radiation belts around 00:00 MLT. Once in the belts, the electrons tend to drift to later magnetic local times and generate chorus waves. However, this is in contradiction with the high wave power shown near the equator *before* 00:00 MLT (top right plot in Figure 7). This region is ordinarily within the plasmapause so we have very few measurements to compare it to. However, it is likely that the filling and smoothing algorithms are overestimating the wavepower here. More work will need to be done in order to ascertain if this an artifact.

The plots also do not contain a model of the magnetopause, which is observed to move inwards on the dayside at high activities. Once the magnetopause position is known, adding it to the plots would simply be a case of deleting all chorus waves outside this radius.

It is instructive to compare the top three dial plots in figure 7 with the measured data in the same region (Figure 2). At $8 \leqslant K_p < 9$ an intensity map has been created where there was previously very little data. The $4 \leqslant K_p < 5$ maps show similar values of intensity and similar distribution patterns, suggesting our extrapolation techniques are well grounded. However, at $0 \leqslant K_p < 1$, the measured wave intensities are around ten times lower than the predicted intensities. This is because the linear fit performs badly in the low K_p region, as discussed in section 4. That being said, the low activity predictions are of less importance, since they will not be used to calculate diffusion coefficients.

Figure 8 shows the frequency distribution of chorus wave power. These spectra show a dip at half of the gyrofrequency ($0.5f_{ce}$), due to a resonance with electrons oscillating at $1f_{ce}$. The wavepower between $0.5f_{ce}$ and $1.0f_{ce}$ (upper band) decreases with increasing L^*. This is a recognised phenomenon, the cause of which is still uncertain [*Meredith et al.,* 2002].

The spectra for $K_p \geqslant 4$ will be used to calculate electron pitch angle and energy diffusion coefficients for simulations of large geomagnetic storms. See [*Horne et al.,* 2013(2)] for a description of this process.

8. Conclusions

Satellite measurements of chorus wave intensity were extrapolated to higher K_p levels using linear fits, and gaps in the data were filled in with surrounding values. This gave maps of chorus wave power throughout the outer radiation belt, at 11 activity levels in the range $0 \leqslant K_p < 10$. The maps are in good agreement with theory and previous observations during periods of high geomagnetic activity. However, the maps tend to overestimate wave intensity during low activities, this could possibly be rectified if exponential fits were used in the low K_p region.

We also require a model of the magnetopause in order to realistically show the outer edge of the radiation belts. Similarly, a case study of events when the plasmapause moves inward to $L^* < 3$ would enable us to better model the inner edge of the radiation belts.

Some suggestions for future research include extrapolating the electromagnetic hiss and plasma frequency measurements, which are also used to model geomagnetic storms. Also, to carry out extrapolations using the AE rather than K_p index.

Acknowledgements. Many thanks to Nigel Meredith and Sarah Glauert for guiding my work. I would also like to thank Richard Horne, Tobias Kersten and Mark Phillips for their explanations. This is a European Union funded project.

References

Baker, D. N., Kanekal, S. G., Li, X., Monk, S. P., Goldstein, J., Burch, J. L., (2004), An extreme distortion of the Van Allen belt arising from the 'Hallowe'en' solar storm in 2003, *Nature, 432*, 878-881.

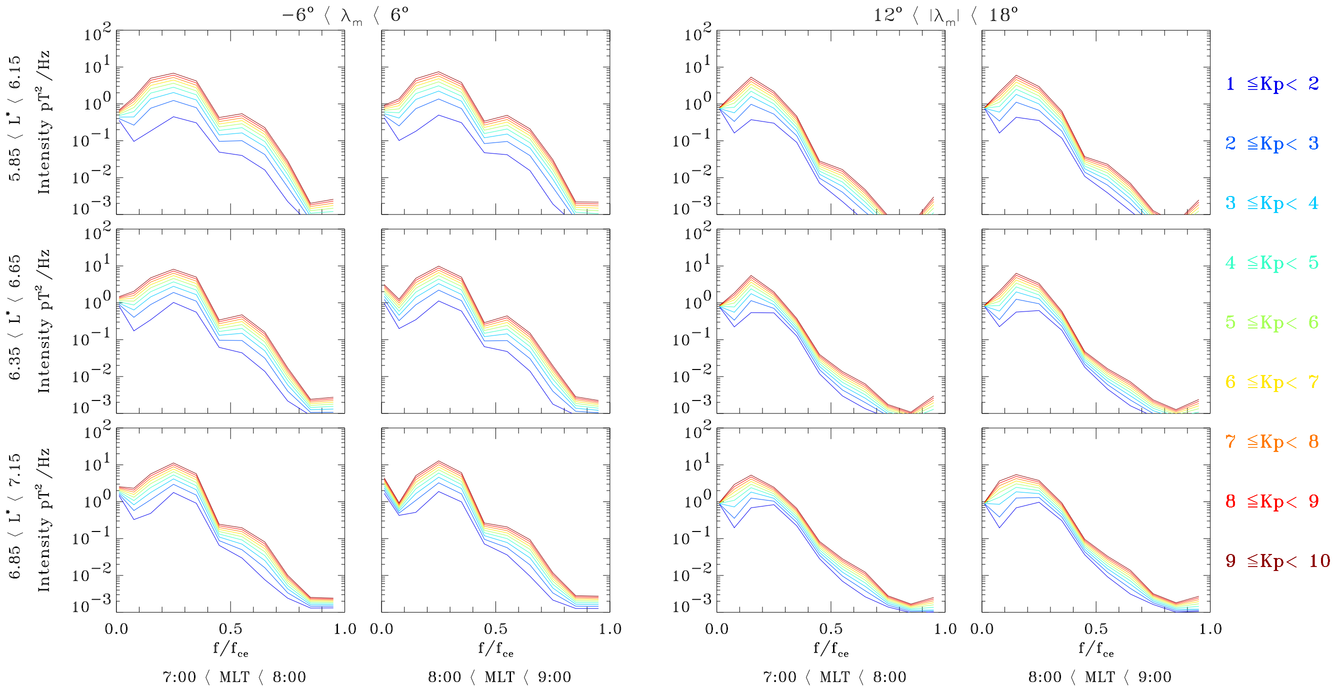

Fig. 8: Chorus wave spectra. The six plots on the left show the spectral content of six bins in the equatorial plane, and those on the right correspond to bins at higher latitudes. Note how the upper band wavepower ($0.5f_{ce} < f < 1.0f_{ce}$) becomes small at large L^* and greater latitudes.

Bortnik, J., Thorne, R. M., & Meredith, N. P., (2007), Modelling the propagation characteristics of chorus using CRRES suprathermal electron fluxes, *J. Geophys. Res., 112*, A08204.

Horne, R. B., Glauert, S. A., Meredith, N. P., Heynderickx, D., & Pitchford, D., (2013), Space weather impacts on satellites and forecasting the Earth's electron radiation belts with SPACECAST, *Space Weather, 11*, 169-186.

Horne, R. B., Kersten, T., Glauert, S. A., Meredith, N. P., Boscher, D., Sicard-Piet, A., Thorne, R. M., & Li, W., (2013), A new diffusion matrix for whistler mode chorus waves, *J. Geophys. Res., 118*, 6302-6318.

Kersten, T., (2016) Electron acceleration and loss caused by wave particle interactions in the Van Allen radiation belts (Doctoral Thesis).

Meredith, N. P., Horne, R. B., Iles, R., Thorne, R., Heynderickx, D., & Anderson, R., (2002), Outer zone relativistic electron acceleration associated with substorm-enhanced whistler mode chorus, *J. Geophys. Res., 107*.

Meredith, N. P., Horne, R. B., Roger, H. A., Thorne, R. M., & Li, W., (2013), A new diffusion matrix for whistler mode chorus waves, *J. Geophys. Res., 118*, 6302-6318.

Satellite Industry Association, (2016), State of the satellite industry report, *sia.org/state-of-the-satellite-industry-report*.

Van Allen, J A., (1959), Geomagnetically trapped corpuscular radiation, *J. Geophys. Res., 64*, 1683-1689.